

Dynamics of two-photon paired superradiance

M. Yoshimura,^{1,*} N. Sasao,^{2,†} and M. Tanaka^{3,‡}

¹*Center of Quantum Universe, Faculty of Science, Okayama University,
Tsushima-naka 3-1-1 Kita-ku, Okayama 700-8530, Japan*

²*Research Core for Extreme Quantum World, Okayama University,
Tsushima-naka 3-1-1 Kita-ku, Okayama 700-8530, Japan*

³*Department of Physics, Graduate School of Science,
Osaka University, Toyonaka, Osaka 560-0043, Japan*

Abstract

We develop for dipole-forbidden transition a dynamical theory of two-photon paired superradiance, or PSR for short. This is a cooperative process characterized by two photons back to back emitted with equal energies. By irradiation of trigger laser from two target ends, with its frequency tuned at the half energy between two levels, a macroscopically coherent state of medium and fields dynamically emerges as time evolves and large signal of amplified output occurs with a time delay. The basic semi-classical equations in 1+1 spacetime dimensions are derived for the field plus medium system to describe the spacetime evolution of the entire system, and numerically solved to demonstrate existence of both explosive and weak PSR phenomena in the presence of relaxation terms. The explosive PSR event terminates accompanying a sudden release of most energy stored in the target. Our numerical simulations are performed using a vibrational transition $X^1\Sigma_g^+ v = 1 \rightarrow 0$ of para- H_2 molecule, and taking many different excited atom number densities and different initial coherences between the metastable and the ground states. In an example of number density close to $O[10^{21}]\text{cm}^{-3}$ and of high initial coherence, the explosive event terminates at several nano seconds after the trigger irradiation, when the phase relaxation time of $> O[10]$ ns is taken. After PSR events the system is expected to follow a steady state solution which is obtained by analytic means, and is made of many objects of field condensates endowed with a topological stability.

PACS numbers: 42.50.Nn, 42.50.Gy, 42.65.Sf

*Electronic address: yoshim@fphy.hep.okayama-u.ac.jp

†Electronic address: sasao@fphy.hep.okayama-u.ac.jp

‡Electronic address: tanaka@phys.sci.osaka-u.ac.jp

I. INTRODUCTION

Since the early suggestion [1] a variety of coherent two-photon processes have attracted much interest, both from theoretical [2], [3], [4] and experimental sides [5], [6], [7], [8], [9]. Our present work is focused on a different aspect of coherent two photon emission from Λ -type three level atoms (or molecules) where transition between two lower levels is dipole-forbidden (see Fig(1) for the level structure). As pointed out in [10], a macroscopic target made of metastable atoms in the $|e\rangle$ of Fig(1) may induce a characteristic event of macro-coherent two photon emission, two photons exactly back to back emitted with equal energies. We use for this phenomenon the terminology of two-photon paired superradiance, or PSR in short. The term paired is used because two emitted photons are highly correlated in their momenta and spin orientations (most clearly seen in $J = 0 \rightarrow 0$ transition). The rate enhancement factor in the momentum configuration of the back to back emission is expected much larger than in the usual superradiance (SR) case [11] due to lack of the wavelength limitation there: the coherent volume for SR is limited with the wavelength λ by $\lambda^2 L$ where L is the target length for a cylindrical configuration, while the macro-coherent PSR has the coherent volume of entire cylinder irradiated by trigger.

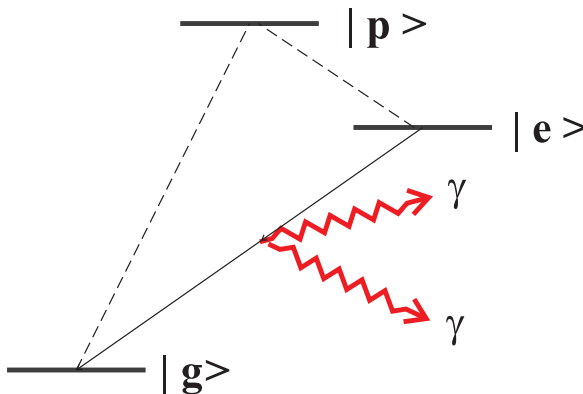


FIG. 1: (Color online) Λ -type atomic level for PSR. Dipole forbidden transition $|e\rangle \rightarrow |g\rangle + \gamma + \gamma$ may occur via strong E1 couplings to $|p\rangle$.

The usual single photon superradiance occurs irrespective of absence or presence of trigger due to the intrinsic instability of exponential spontaneous decay caused by dipole-allowed transition. On the other hand, two-photon emission occurs with a much smaller rate in higher order of perturbation beyond dipole-forbidden transition, hence the use of trigger

is essential to assist the macro-coherence development for two-photon process and induce rapid PSR events of large signal. Quantum initiation such as proposed for SR in [12] is not needed, since PSR is more akin to the triggered SR [13], which makes appropriate the following semi-classical treatment.

A basic formalism of two-photon process already exists, [3] for propagation equation and [14] for analytic results of the propagation problem and PSR emission treated as perturbation. But this formulation turns out insufficient to dynamically discuss two (back to back) mode propagation incorporating PSR, which seems essential for dense medium. In the present work we shall be able to derive a fundamental set of semi-classical equations for the two mode and further present formulation of two color problem as well. The essential ingredient in our work is derivation of a more general quantum mechanical equation both for the medium (Bloch equation) and the electromagnetic field (extension of quantum Maxwell equation to include two photon process). Only after elucidating the nature of quantum state of fields and medium, namely, time evolving electric field condensate, we shall go on to the semi-classical equation. This way we determine how two back to back modes are precisely coupled beyond the perturbation theory.

We ignore the granularity and rely on the continuum limit formulation of atom distribution, taking one spatial dimension alone, because the whole event is highly focused on one direction of irradiated trigger field taken as x direction. The system of semi-classical partial differential equations thus derived is highly non-linear, and must generally be analyzed by numerical simulations. This way we find explosive and weak PSR phenomena and under what conditions these may occur.

Despite of its complicated non-linearity the system allows soliton solution of two kinds, which is obtained as steady state solutions of this non-linear system of fields and medium. Solitons here, in their field part, are electric field condensate which may or may not be moving: there can be static field condensate. The stability (against two-photon emission) of solitons is ensured by a topological quantum number as explained in the text below. Our conjecture, which is supported by numerical simulations, but not established by a more rigorous method, is that field condensate formed after rapid PSR phenomena is made of many topological solitons. After formation of field condensates, namely a stable target state against two photon emission, the light may propagate almost freely. The condensate state of field plus medium thus formed may be very useful to detect a much weaker process such as

radiative neutrino pair emission (RNPE) [15], because the condensate is not stable against RNPE.

A related propagation and soliton formation problem in the single photon case is the phenomenon of self-induced transparency (SIT) [16] and electromagnetically induced transparency (EIT) [8] presumably related to solitons of the kind of [17], both at a resonant frequency. Both of these transparency phenomena thus appear to be directly related to formation of stable solitons of different kinds from ours.

For numerical computations below, we use parameters relevant to a good target candidate for PSR detection, para-H₂ molecule. We have in mind using para-H₂ vibrational transition of $X^1\Sigma_g^+ v = 1 \rightarrow 0$ (X being the electronically ground molecular state). Many other atoms and molecules are conceivable for PSR experiments. The characteristic length scale for large effects is $\sim 14\text{cm}$, and the time scale $\sim 0.5\text{ ns}$ for para-H₂ of a molecule density of $n = 10^{20}\text{cm}^{-3}$. The number density dependence of these characteristic parameters is $\propto 1/n$. We include relaxation effects of two time constants in the range of $T_2 \geq 10\text{ ns}$ (a feasible value experimentally) and $T_1 \gg T_2$ in our analysis. Origin of these relaxation constants is left unexplained, and this way one may use values experimentally measured by other means. We perform extensive numerical simulation in order to clarify experimentally observable PSR signals and condensate formation in forthcoming experiments. It is demonstrated that explosive PSR emission occurs for long targets even by weak trigger when initial coherence between states, $|e\rangle$ and $|g\rangle$, is present. We have identified two different types of PSR events caused by trigger irradiation: (1) explosive PSR in which most of the stored energy in the initial metastable state $|e\rangle$ is released as a short pulse of some time structure, and (2) weak PSR in which the output energy flux is in linear proportion to the trigger power.

The natural unit $\hbar = c = 1$ is used throughout in the present paper.

II. DERIVATION OF QUANTUM AND SEMI-CLASSICAL EQUATION

Consider three level atom (or molecule) of energies, $\epsilon_p > \epsilon_e > \epsilon_g$, as shown in Fig(1). We assume that transition between two lower levels, $|e\rangle$ and $|g\rangle$, are dipole forbidden. Suppose that the upper level $|p\rangle$ has substantial E1 rates both to $|e\rangle, |g\rangle$. (This can be replaced by weaker M1 transition, since the relation we need subsequently is the partial decay rate $\propto \epsilon_{ij}^3$ with the energy level difference $\epsilon_{ij} = \epsilon_i - \epsilon_j$, which holds both in E1 and M1 cases.)

We focus on, and derive an effective hamiltonian of, two lower levels interacting with oscillating electric field E . Its hamiltonian density has been derived in [3], [14] for a single mode of field such as a light wave of definite frequency traveling in one direction. Extension to multi-mode fields such as counter-propagating modes of the same frequency is given in Appendix A. Its hamiltonian has a form of 2×2 matrix acting on two atomic states, $|e\rangle$ and $|g\rangle$, $\sim E^T \mathcal{M} E$. The multi-mode field E may be decomposed into positive and negative frequency parts $E^T = \sum_j \frac{1}{2}(E_j^* e^{i\omega_j t} + E_j e^{-i\omega_j t})$, where E_j, E_j^* are slowly varying envelopes in time. We shall use variables, $E_j^+ = E_j e^{-i\omega_j t}$, $E_j^- = E_j^* e^{i\omega_j t}$, to simplify formulas given below. In quantum field theory E_j and E_j^* represent annihilation and creation operators of definite mode. The pertinent hamiltonian to our discussion of the single mode is

$$\frac{d}{dt} \begin{pmatrix} c_e(x, t) \\ c_g(x, t) \end{pmatrix} = -i\mathcal{H}_I \begin{pmatrix} c_e(x, t) \\ c_g(x, t) \end{pmatrix}, \quad (1)$$

$$-\mathcal{H}_I = \begin{pmatrix} \mu_{ee} E^+ E^- & e^{i\epsilon_{eg} t} \mu_{ge} (E^+)^2 \\ e^{-i\epsilon_{eg} t} \mu_{ge} (E^-)^2 & \mu_{gg} E^+ E^- \end{pmatrix}, \quad (2)$$

$$\mu_{ge} = \frac{2d_{pe}d_{pg}}{\epsilon_{pg} + \epsilon_{pe}}, \quad \mu_{aa} = \frac{2d_{pa}^2 \epsilon_{pa}}{\epsilon_{pa}^2 - \omega_0^2}, \quad (a = g, e), \quad (3)$$

where $|c_e|^2 + |c_g|^2 = n(x)$ with $n(x)$ the number density of atoms per a unit volume in a linear target region of $0 \leq x \leq L$. For simplicity we took isotropic medium and linearly polarized fields, taking \vec{E}^\pm as scalar functions. The diagonal part $\propto \mu_{aa}$ of this hamiltonian describes AC Stark energy shifts, while off-diagonal parts $\propto \mu_{ge}$ are for two photon emission and absorption.

For pH₂ target the photon energy $\omega_0 = \epsilon_{eg}/2 \sim 0.26$ eV is much smaller than level spacings to the electronically excited intermediate states, both ϵ_{pe} and $\epsilon_{pg} \sim 11$ eV. Under this condition we may ignore ω_0 compared to ϵ_{pa} , $a = e, g$ in the formula for μ_{ab} and identify μ_{ab} to the polarizability for which precision calculation exists [18]. We thus use numerical values of parameters, $\mu_{gg} \sim 0.80$, $\mu_{ee} \sim 0.87$, $\mu_{ge} \sim 0.055$ all in the unit of 10^{-24} cm³ [19] for the pH₂ $Xv = 1 \rightarrow Xv = 0$ transition.

The density matrix of pure atomic states, $\rho = |\psi(x, t)\rangle\langle\psi(x, t)|$ ($|\psi(x, t)\rangle = (c_e, c_g)$), obeys the evolution equation, $\partial_t \rho = -i[\mathcal{H}_I, \rho]$. This quantum mechanical equation is generalized to include dissipation or relaxation. The needed variable, the density matrix for the mixed

state, is given by a statistical mixture of pure states:

$$\rho(x, t) = \sum_i c_i |\psi_i(x, t)\rangle \langle \psi_i(x, t)|, \quad \sum_i c_i = 1, \quad 0 \leq c_i \leq 1, \quad (4)$$

with $|\psi_i(x, t)\rangle$ a set of orthonormal pure state vectors. Dissipation occurs when a subsystem of $|e\rangle, |g\rangle$ interacts with a reservoir and one integrates out reservoir variables due to our basic ignorance of the reservoir. The general form of mixed state evolution including dissipation has been derived by Lindblad [20], assuming the general principle of positivity and conservation of probability. As its result the time evolution equation of the density matrix has additional operator term, $L[\rho]$. The new additional dissipation term in the two level atomic system turns out equivalent to phenomenological relaxation terms given by two time constants, T_1, T_2 (with the constraint $T_1 > T_2/2$ from consistency with [20]).

It is convenient to write the evolution equations in terms of components of the Bloch vector defined by $\vec{R} = \text{tr } \rho \vec{\sigma} = \langle \psi | \vec{\sigma} | \psi \rangle$. The basic Bloch equation including relaxation terms is

$$\partial_t R_1 = (\mu_{ee} - \mu_{gg}) E^+ E^- R_2 - i \mu_{ge} (e^{i\epsilon_{eg}t} E^+ E^+ - e^{-i\epsilon_{eg}t} E^- E^-) R_3 - \frac{R_1}{T_2}, \quad (5)$$

$$\partial_t R_2 = -(\mu_{ee} - \mu_{gg}) E^+ E^- R_1 + \mu_{ge} (e^{i\epsilon_{eg}t} E^+ E^+ + e^{-i\epsilon_{eg}t} E^- E^-) R_3 - \frac{R_2}{T_2}, \quad (6)$$

$$\partial_t R_3 = \mu_{ge} (i(e^{i\epsilon_{eg}t} E^+ E^+ - e^{-i\epsilon_{eg}t} E^- E^-) R_1 - (e^{i\epsilon_{eg}t} E^+ E^+ + e^{-i\epsilon_{eg}t} E^- E^-) R_2) - \frac{R_3 + n}{T_1}. \quad (7)$$

$T_1 \gg T_2$ usually, and the phase decoherence time T_2 is much smaller and more important than the decay time T_1 , which may be taken infinitely large for our practical purpose.

Derivation of quantum field equation follows a similar line of reasonings. To perform the derivative operation ∂_t^2 as in the Maxwell equation, one needs to calculate the double commutator;

$$\partial_t^2 \vec{E}^\pm = -[H, [H, \vec{E}^\pm]], \quad H = \int d^3x (\mathcal{H}_f + \text{tr } \rho \mathcal{H}_I), \quad (8)$$

with the field energy density $\mathcal{H}_f = (\vec{E}^2 + \vec{B}^2)/2$. For convenience we add less dominant oscillating terms of field modes to E^\pm and use the locally well behaved field $E(x, t)$ in \mathcal{H}_I . The fundamental commutation relation in the radiation gauge QED $[E_y(\vec{r}, t), B_z(\vec{r}', t)] = i\partial_x \delta^3(\vec{r} - \vec{r}')$ [21] is used for derivation of quantum field equation. The result is

$$(\partial_t^2 - \vec{\nabla}^2) \vec{E}^\pm = \vec{\nabla}^2 \mathcal{D} \vec{E}^\pm, \quad (9)$$

$$-\mathcal{D} \vec{E}^+ = \left(\frac{\mu_{ee} + \mu_{gg} n}{2} + \frac{\mu_{ee} - \mu_{gg} R_3}{2} \right) \vec{E}^+ + \mu_{ge} e^{-i\epsilon_{eg}t} (R_1 - iR_2) \vec{E}^-. \quad (10)$$

This equation [22] along with the Bloch equations (5)~ (7) is the basis of the following derivation of our master equation.

Slowly Varying Envelope Approximation (SVEA) Fast oscillating terms do not contribute to global features of time and spatial evolution when one makes averaging over a few \times time and spatial oscillation periods. We thus extract terms that persist over time periods of typical light oscillation of order $1/\omega$ both in time and space. Envelope functions denoted by E_R, E_L ought to be amplitudes of right and left moving components of rapidly oscillating parts $\propto e^{-i\omega(t\mp x)}$.

The result of SVEA may be summarized using dimensionless units of spacetime coordinates ξ, τ and dimensionless fields $e_{L,R}$ given by

$$(\xi, \tau) = (\alpha_m x, \alpha_m t), \quad \alpha_m(\omega) = \frac{\epsilon_{eg}}{2} n \mu_{ge}(\omega), \quad |e_{L,R}|^2 = \frac{|E_{L,R}|^2}{\epsilon_{eg} n}, \quad r_i = \frac{R_i}{n}. \quad (11)$$

The quantity $1/\alpha_m = 2/(\mu_{ge}\epsilon_{eg}n)$ gives a fundamental unit of target length and time scale of evolution. Since a functional relation $\alpha_m(\omega) = \alpha_m(\epsilon_{eg} - \omega)$ holds, the propagation problem of trigger irradiation of pair frequencies, ω and $\epsilon_{eg} - \omega$, is described by the same dimensionless quantities of a common α_m . Its value at $\omega = \epsilon_{eg}/2$ is $\sim 14\text{cm}$ and $\sim 0.5\text{ ns}$ for para-H₂ of density 10^{20}cm^{-3} .

The most general fundamental equations including both non-trivial propagation and PSR effects are derived in Appendix A and given by the formulas (A35) ~ (A42). It is useful to recall the physical meaning of coupling constants μ_{ab} in the interaction hamiltonian, in order to fully appreciate the following approximation in our numerical simulations. Consider the extended hamiltonian including both of counter-propagating modes given by eq.(A14) in Appendix. We first note that annihilation (a_i) and creation (a_i^\dagger) operators of photon modes are related to complex fields by $E_i^+ \sim a_i \sqrt{\omega/2V}, E_i^- \sim a_i^\dagger \sqrt{\omega/2V}$ where V is the quantization volume. The important equations are obtained after SVEA and given in

Appendix A. They are written in terms of envelope functions:

$$(\partial_t + \partial_x)E_R = \frac{i\omega}{2} \left(\left(\frac{\mu_{ee} + \mu_{gg}}{2} n + \frac{\mu_{ee} - \mu_{gg}}{2} R_3^{(0)} \right) E_R + \frac{\mu_{ee} - \mu_{gg}}{2} R_3^{(+)} E_L \right. \\ \left. + \mu_{ge} \left((R_1 - iR_2)^{(0)} E_L^* + (R_1 - iR_2)^{(+)} E_R^* \right) \right), \quad (12)$$

$$(\partial_t - \partial_x)E_L = \frac{i\omega}{2} \left(\left(\frac{\mu_{ee} + \mu_{gg}}{2} n + \frac{\mu_{ee} - \mu_{gg}}{2} R_3^{(0)} \right) E_L + \frac{\mu_{ee} - \mu_{gg}}{2} R_3^{(-)} E_R \right. \\ \left. + \mu_{ge} \left((R_1 - iR_2)^{(0)} E_R^* + (R_1 - iR_2)^{(-)} E_L^* \right) \right). \quad (13)$$

The right hand sides of these equations give effects, all in bulk medium, of forward scattering $\propto \frac{\mu_{ee} + \mu_{gg}}{2} n + \frac{\mu_{ee} - \mu_{gg}}{2} R_3^{(0)}$, backward scattering $\propto \frac{\mu_{ee} - \mu_{gg}}{2} R_3^{(\pm)}$, RL-pair annihilation $\propto \mu_{ge} (R_1 - iR_2)^{(0)}$, and RR-, LL-pair annihilation $\propto \mu_{ge} (R_1 - iR_2)^{(\pm)}$. (The pair creation amplitudes appear in conjugate equations to those above.) Quantities $R_i^{(\pm)} e^{\pm 2ikx}$ as defined by eq.(A31) are what are called spatial grating in the literature. The backward scattering terms, and RR-, LL-pair annihilation and creation terms are important only in the presence of spatial grating of polarization. Neglect of spatial grating is thus equivalent to retaining forward scattering and RL-pair processes, and ignoring all other terms. In the simple boundary condition set up below in this work, the backward Bragg scattering is expected to be a minor effect, and is also neglected in most works of SR. We refer to [23] on the backward Bragg scattering effect in usual SR, and for instance to [24] on the backward scattering effect on SR in low-Q cavity experiments. In a more comprehensive simulation in future we wish to quantitatively compute effects of the backward scattering, RR-, LL-pair processes, because non-negligible differences of these effects might arise in PSR unlike the SR case.

In the rest of the present work we shall focus on PSR effects and ignore propagation effects which are much discussed in [3], [14] and summarized in Appendix A. Explosive PSR events discussed below are expected to be insensitive to neglected propagation effects. The resulting Maxwell-Bloch equation for the single mode is

$$\partial_\tau r_1 = 4\gamma_- (|e_R|^2 + |e_L|^2) r_2 + 8\Im(e_R e_L) r_3 - \frac{r_1}{\tau_2}, \quad (14)$$

$$\partial_\tau r_2 = -4\gamma_- (|e_R|^2 + |e_L|^2) r_1 + 8\Re(e_R e_L) r_3 - \frac{r_2}{\tau_2}, \quad (15)$$

$$\partial_\tau r_3 = -8 (\Re(e_R e_L) r_2 + \Im(e_R e_L) r_1) - \frac{r_3 + 1}{\tau_1}, \quad (16)$$

$$(\partial_\tau + \partial_\xi)e_R = \frac{i}{2}(\gamma_+ + \gamma_- r_3)e_R + \frac{i}{2}(r_1 - ir_2)e_L^*, \quad (17)$$

$$(\partial_\tau - \partial_\xi)e_L = \frac{i}{2}(\gamma_+ + \gamma_- r_3)e_L + \frac{i}{2}(r_1 - ir_2)e_R^*, \quad (18)$$

$$\gamma_\pm = \frac{\mu_{ee} \pm \mu_{gg}}{2\mu_{ge}}. \quad (19)$$

Here $\tau_i = \alpha_m T_i$ are relaxation times in the dimensionless unit.

The dimensionless master equation (14) ~ (18) is governed by two important parameters, the most important is $\tau_2 = \alpha_m T_2$ and the next important is γ_\pm . Another experimentally important parameter is the overall length and time $1/\alpha_m \propto 1/n$, inversely scaling with the number density n . For larger number densities of excited atoms a smaller size target and a shorter time measurement of O[ns] becomes possible.

In terms of two component field φ defined below the equation reads as

$$(\partial_\tau + \sigma_3 \partial_\xi)\varphi = \frac{i}{2}(\gamma_+ + \gamma_- r_3)\varphi + \frac{i}{2}(r_1 - ir_2)\sigma_1\varphi^*, \quad \varphi = \begin{pmatrix} e_R \\ e_L \end{pmatrix}. \quad (20)$$

Magnitudes of R- and L-fluxes change via RL mixing term such as

$$(\partial_\tau \pm \partial_\xi)|e_{R,L}|^2 = r_1 \Im(e_R e_L) + r_2 \Re(e_R e_L). \quad (21)$$

R- or L-moving pulse alone propagates freely, because we ignored in this approximation non-trivial propagation effects.

Quantum state of fields As usual in quantum field theory, we may interpret $\vec{E}_{R,L}$ as annihilation and $\vec{E}_{R,L}^\dagger$ as creation operator. The fact that the basic equation, (17) ~ (18) or (20), simultaneously contains both annihilation and creation operators of field implies that the quantum state satisfying the field equation is given by a Bogoliubov transformation from the usual vacuum of zero photon state $|0\rangle$,

$$|\Psi\rangle = \sum_{n=0}^{\infty} c_n(x, t) (E_R^\dagger E_L^\dagger)^n |0\rangle, \quad (22)$$

where $c_n(x, t)$ is to be determined by (eq.(20)) $|\Psi\rangle = 0$. The quantum state $|\Psi\rangle$ is a mixture of infinitely many states of different photon number. We shall not pursue this line of thoughts any further, because we exploit the semi-classical approximation under the large quantum number limit of photons (the classical limit). The semi-classical equation is given by the

expectation value of quantum equation,

$$\langle \Psi | \left((\partial_\tau + \sigma_3 \partial_\xi) \varphi - \frac{i}{2} (\gamma_+ + \gamma_- r_3) \varphi - \frac{i}{2} (r_1 - ir_2) \sigma_1 \varphi^* \right) | \Psi \rangle = 0, \quad (23)$$

with $|\Psi\rangle$ the Bogoliubov state given by eq.(22). The semi-classical equation turns out equivalent to replacing q-field operators in the quantum equation by corresponding c-number functions. Equations, (14) \sim (18), regarded as equations for c-number functions, thus constitute the master equation for polarization of medium and field.

In our case of field condensate, medium polarization and fields are cooperatively involved: the target medium undergoes coherence oscillation, simultaneous with field oscillation, while keeping field envelopes slowly varying and finally almost time independent in a large time limit, as shown below. The field condensate part is technically equivalent to field state made of an infinite sum of multiple photon pair states in the so-called coherent state representation.

III. IMPORTANCE OF INITIAL COHERENCE

It is important to clarify in detail the ideal case of numerical solutions where all quantities in eq.(14) \sim (18) are of order unity, in the range of $O[10 \sim 1/10]$. For a deeper understanding of numerical outputs and a practical check of accuracy of numerical results, it is useful to know conservation laws of our non-linear system. We list in Appendix B all exact and approximate conservation laws that the system possesses.

We have performed numerical simulations assuming CW (non-pulsed continuous wave) trigger laser irradiation of the same power from two target ends (called the symmetric trigger). This boundary condition is similar, but not identical, to the one of cavity mirror. Use of cavity mirrors has both advantage and complication. Two mirrors in cavity automatically generate counter-propagating waves, and they effectively increase the trigger power (which however is not critically needed in our case). On the other hand, each atom in cavity is affected by the same traveling fields many times and this complicates analysis. We use in the present work the simpler scheme of two CW counter-propagating triggers independently irradiated.

Numerical results show the symmetric output fluxes from two ends, and we exhibit in the following figures one of these identical fluxes from one end. Result for the zero initial coherence $r_1(\xi, 0) = r_2(\xi, 0) = 0$ is shown in Fig(2). Clear signature of delay much after T_2

($\sim 7T_2$ in this case) and explosive PSR is observed for strong trigger fields. It is difficult to obtain commercially available CW laser of this power. A reason of this difficulty is that relaxation of order $T_2 \sim 10\text{ns}$ may take over the coherence development under weak trigger usually exploited. Explosive PSR is a highly non-linear process having a definite trigger power threshold and disappears in this example certainly at the trigger power of 0.9 MWmm^{-2} , as shown in the inset of Fig(2).

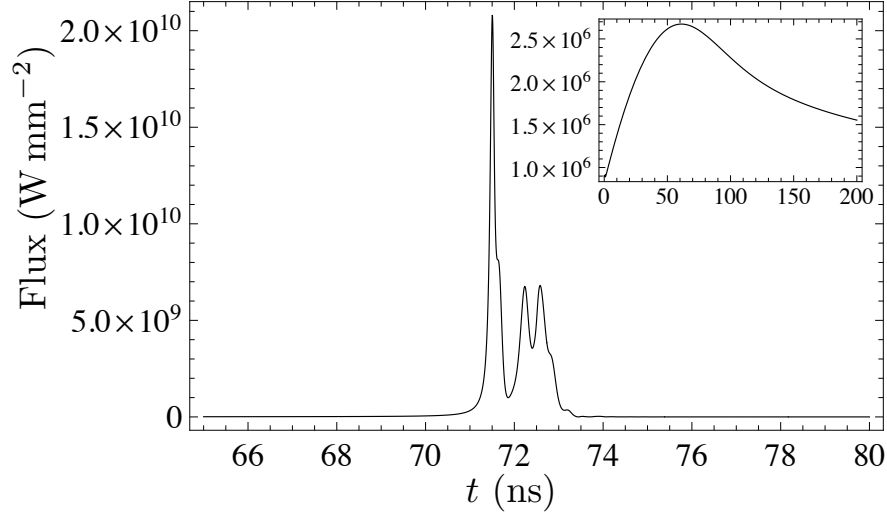


FIG. 2: Time evolving output flux at a target end of length 30 cm resulting from the symmetric CW trigger irradiation of power 1 MW mm^{-2} and 0.9 MW mm^{-2} in the inset. (Note a large difference of $\sim 10^4$ of the output power in two plots.) Assumed parameters are $n = 1 \times 10^{21} \text{ cm}^{-3}$ of pH_2 , numerical values (see the text) of μ_{ab} for the transition $Xv = 1 \rightarrow Xv = 0$, relaxation times $T_2 = 10$, $T_1 = 10^3$ ns's, and initial complete inversion (hence no coherence) of $r_3 = 1$ with $r_1, r_2 = 0$ taken for the initial target state.

In Fig(2) the complete inversion to the level $|e\rangle$ has been assumed as an initial condition, and it would be interesting to relax this condition and to further clarify neglected effects of the presence of initial coherence between two atomic levels, $|e\rangle$ and $|g\rangle$. There is an experimental method to imprint an initial coherence between $|e\rangle$ and $|g\rangle$ by adopting a clever excitation scheme. The atomic state right after excitation can be made a coherent mixture of two pure states, $|e\rangle$ and $|g\rangle$, namely $c_e|e\rangle + c_g|g\rangle$ with $|c_e|^2 + |c_g|^2 = 1$ at a single atomic site, by using the technique of STIRAP [25]. This kind of pure state may be formed by time overlapping excitation pulses of two frequencies, $\approx \epsilon_{pe}$ and $\approx \epsilon_{pg}$. The state is a dark state, called so because no emission from $|p\rangle$ is observed despite of irradiation capable

of making both transitions, $|p\rangle \rightarrow |e\rangle$ and $|p\rangle \rightarrow |g\rangle$.

The medium polarization r_i in the dark state is given by

$$r_1 = 2\sqrt{p(1-p)} \cos \theta_0, \quad r_2 = 2\sqrt{p(1-p)} \sin \theta_0, \quad r_3 = 2p - 1, \quad (24)$$

with p the fraction in the state $|e\rangle$. When this type of initial polarization of the dark state is formed, one may expect to expedite the coherence development for PSR, as shown in the following section. When CW laser is used for trigger, two overlapping pulses may induce PSR at the same time when the emission from $|p\rangle$ disappears: thus it may be called PSR from the dark.

IV. NUMERICAL SOLUTIONS FOR HIGH DENSITY TARGET WITH INITIAL COHERENCE

We first comment on what the number density n of target precisely means. This is the total number of atoms/molecules per a unit volume participating in PSR phenomena, hence it is the added sum of densities in the states, $|e\rangle$ and $|g\rangle$. Note also that the state $|g\rangle$ may or may not be the ground state of atoms or molecules. For instance, in the pH_2 transition of $X^1\Sigma_g^+ v = 2 \rightarrow 1$, the target number density n may be much less than the ground state number density since $|g\rangle = (Xv = 1)$ is also an excited state.

Time evolution from a dark state of initial polarization value given by eq.(24) is illustrated for the pH_2 number density $1 \times 10^{21} \text{cm}^{-3}$ in Fig(3) \sim Fig(11). We exhibit dependence of the symmetric output pulse on the trigger power in the range of $10^{-12} \sim 1 \text{Wmm}^{-2}$ for $n = 1 \times 10^{21} \text{cm}^{-3}$ in Fig(3), which demonstrates two important features of explosive PSR with the presence of a large initial coherence: (1) the highest peak of PSR output is almost independent of the trigger power, suggesting a sudden, macroscopic release of energy (its density $\approx \epsilon_{eg}n$) stored between two levels, $|e\rangle$ and $|g\rangle$, (2) the onset time of explosive events, which may be called the delay time, depends on the input trigger power very weakly, and a linear logarithmic dependence has been confirmed up to 1pW mm^{-2} (instantaneous enhancement factor $\sim 8 \times 10^{21}$ in this case). A similar logarithmic power dependence of the delay time has been observed in numerical simulations of the single photon superradiance when the system is subjected to the trigger.

The integrated flux is $\sim |E_{\text{max}}|^2 \Delta t$ with Δt the time width of explosive event. $|E_{\text{max}}|^2 =$

$O[\epsilon_{eg}n]$ and this integrated flux is estimated as $O[1/\mu_{ge}]$, a quantity independent of the target number density n , if the explosive event occurs. These figures show dramatic effects of initial coherence of the dark state. Observation of explosive events requires a target length $\gg 1/\alpha_m \propto 1/n$.

Detailed time structure of pulses as observed in Fig(3) may differ if one adopts different available experimental parameters, but the output release of energy flux of order $\epsilon_{eg}n$ is universal in explosive PSR events.

Spatial profiles of field fluxes and polarization components, r_i , within the target are illustrated in Fig(4) ~ Fig(11). In this parameter set, about $\sim 30\%$ of the stored energy $\epsilon_{eg}n$ (the corresponding flux unit being $1.2 \times 10^9 \text{ Wmm}^{-2}(n/10^{21}\text{cm}^{-3})$) still remains in the target much after explosive PSR, and we observe a seemingly stable target state. Note that dimensionless fields $|e_i|^2 = |E_i|^2/(\epsilon_{eg}n)$ are plotted in Fig(4) and Fig(5).

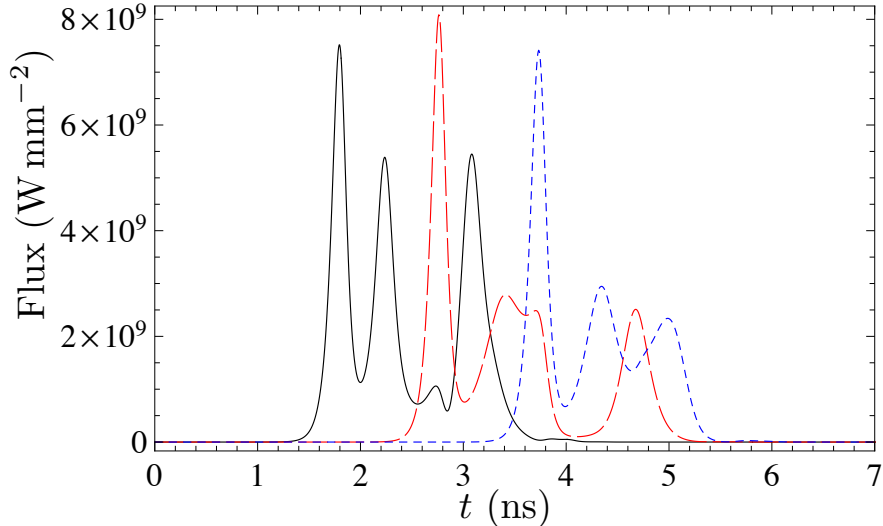


FIG. 3: (Color online) Trigger power dependence of time-evolving output flux from the symmetric trigger irradiation of the power range, $10^{-12} \sim 1 \text{ Wmm}^{-2}$, under the conditions of $n = 1 \times 10^{21} \text{ cm}^{-3}$, target length = 30cm, relaxation times $T_2 = 10, T_1 = 10^3$ ns's, and the initial polarization, $r_1 = 1, r_2 = r_3 = 0$. Depicted outputs from 1 Wmm^{-2} trigger power in solid black, from 10^{-6} Wmm^{-2} in dashed red, and from $10^{-12} \text{ Wmm}^{-2}$ in dotted blue are displaced almost equi-distantly in the first peak positions. Transition $Xv = 1 \rightarrow Xv = 0$ of pH_2 is considered. $\sim 70\%$ stored energy in the initial metastable state is released in these cases.

Result for the solid density of $n = 2.6 \times 10^{22} \text{ cm}^{-3}$ and smaller excitation of $r_3 \approx -1$ is shown in Fig(12). There is a threshold of the excitation fraction of $|e\rangle$, located between 0.2

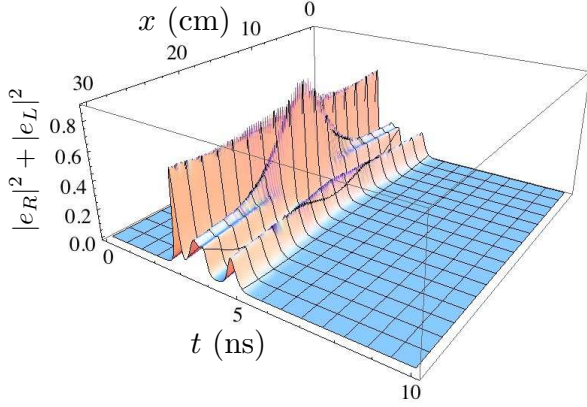


FIG. 4: (Color) Spacetime profile of dimensionless field energy, $|e_R|^2 + |e_L|^2$ for the $1 \mu\text{Wmm}^{-2}$ case of Fig(3).

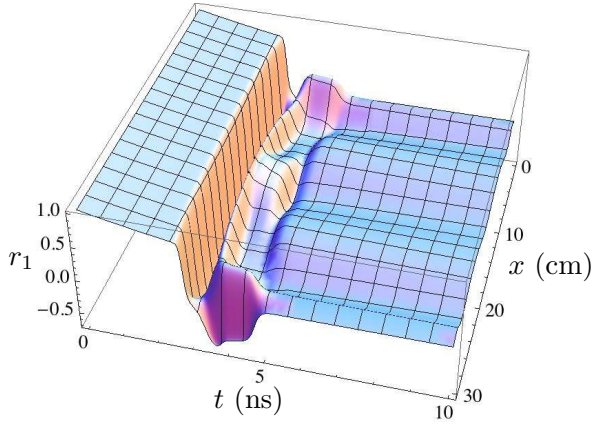


FIG. 6: (Color) Spacetime profile of r_1 for the $1 \mu\text{Wmm}^{-2}$ case of Fig(3).

$\% \sim 0.5 \%$, above which dramatic explosive PSR's emerge, as inferred from comparison of two plots of Fig(12).

So far we mostly showed explosive outputs in which most of the stored energy between $|e\rangle$ and $|g\rangle$ is released in a short time $< 10\text{ns}$ after time delay. There is however a linear regime under a large initial coherence $r_i, i = 1, 2$ in which the output flux is amplified in proportion to the trigger power. For instance, the amplification factor is $\sim 10^2$ in the trigger power range of $1 \mu\text{Wmm}^{-2} \sim 1 \text{Wmm}^{-2}$ for three different choices of initial r_i values of Fig (13). In this figure we show the output fluxes in the linear regime taking as an example the

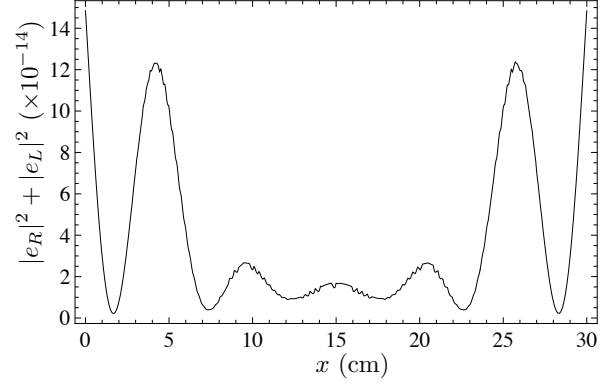


FIG. 5: Spatial profile at the latest time, 10 ns after trigger irradiation, of Fig(4). Note a large reduction by $O[10^{-13}]$ in the power scale in this figure.

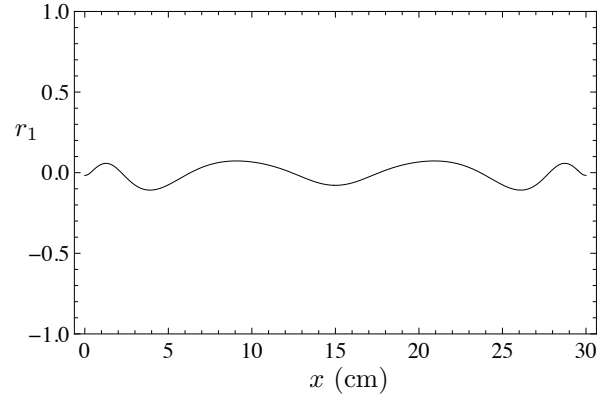


FIG. 7: Spatial profile of r_1 at the latest time, 10 ns after trigger irradiation, of Fig(6).

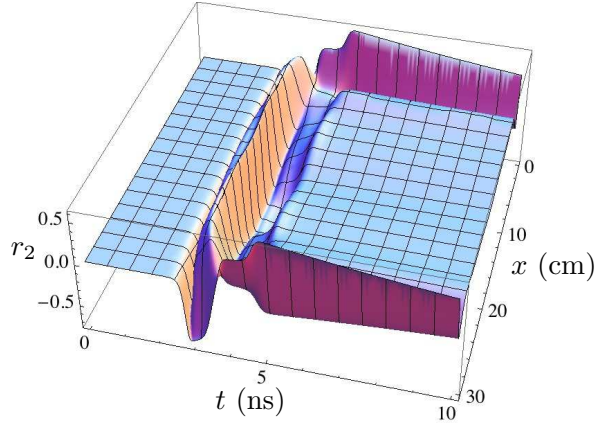


FIG. 8: (Color) Spacetime profile of r_2 for the $1 \mu\text{Wmm}^{-2}$ case of Fig(3).

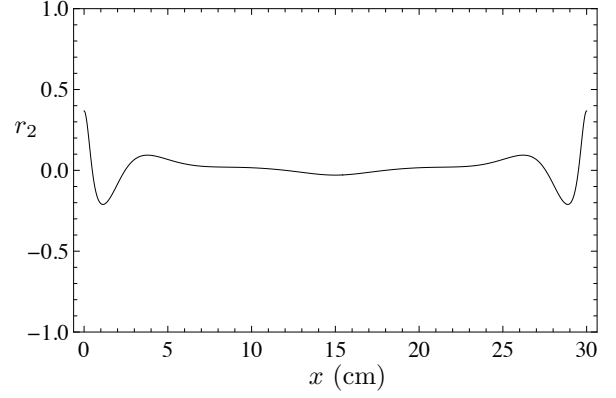


FIG. 9: Spatial profile of r_2 at the latest time, 10 ns after trigger irradiation, of Fig(8).

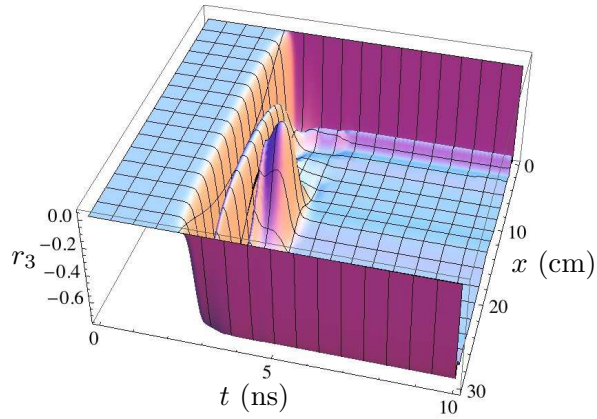


FIG. 10: (Color) Spacetime profile of r_3 for the $1 \mu\text{Wmm}^{-2}$ case of Fig(3).

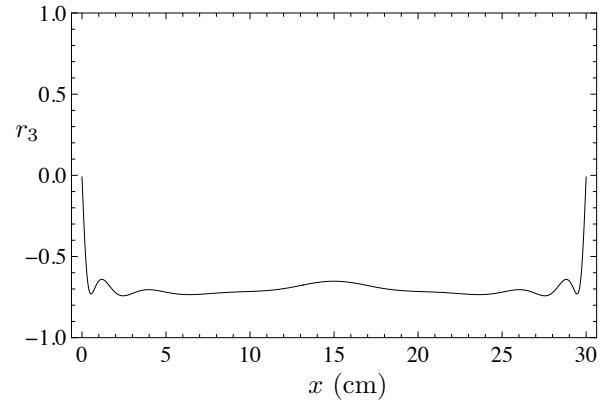


FIG. 11: Spatial profile of r_3 at the latest time, 10 ns after trigger irradiation, of Fig(10).

trigger power of 1 mWmm^{-2} . Although not shown in this figure, the linearity of the output power to the trigger power has been checked for this set of parameters.

V. STATIC REMNANT AND SPINORIAL SOLITONS

In addition to dramatic explosive PSR emission it is also important to watch remnants after PSR emission, since previous figures at latest times may be taken to suggest formation of objects of non-trivial spatial profiles. Let us derive for this purpose the asymptotic form of fundamental equations. We anticipate that both the medium polarization \vec{r} and fields e_R, e_L little change with time in the time region of $t \gg 1/\alpha_m$ after PSR emission. By taking

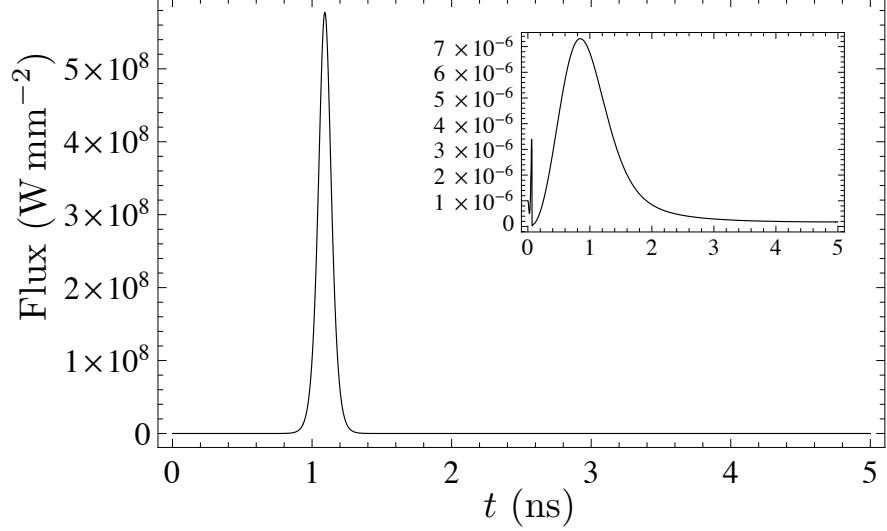


FIG. 12: Output flux for the solid target number density $2.6 \times 10^{22} \text{ cm}^{-3}$ of length 2 cm, the trigger power $1 \mu\text{Wmm}^{-2}$, relaxation times $T_2 = 10, T_1 = 10^3$ ns's, and smaller population $r_3 = -0.99$ (0.5% excitation), and $r_3 = -0.996$ (0.2% excitation) in the inset. The other initial components are taken as $r_1 = \sqrt{1 - r_3^2}$, $r_2 = 0$. Note a large flux scale difference $\sim 10^{14}$ in two plots.

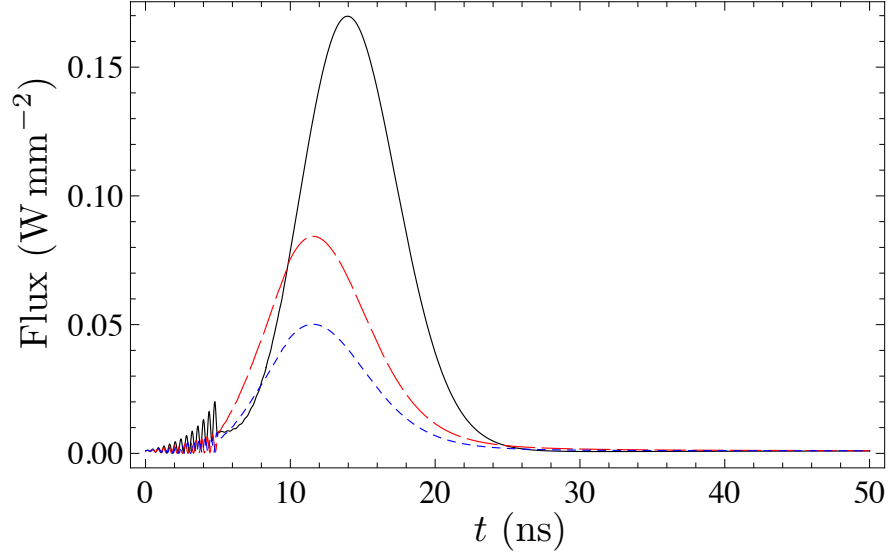


FIG. 13: (Color online) Output flux of weak pH₂ PSR in the linear regime in which the output power $\sim O[10^2] \times$ the trigger power, for initial $(r_3, r_1, r_2) = (0, 1, 0)$ in solid black, $(1/\sqrt{2}, 1/\sqrt{2}, 0)$ in dashed red and $(-1/\sqrt{2}, 1/\sqrt{2}, 0)$ in dotted blue, using the same set of other parameters: $n = 1 \times 10^{20} \text{ cm}^{-3}$, target length = 1.5 m, relaxation times $T_2 = 10, T_1 = 10^3$ ns's, and the trigger power 1 mWmm^{-2} . The output power scales with the trigger power, as explicitly checked in the range of $1 \mu\text{Wmm}^{-2} \sim 1 \text{ Wmm}^{-2}$.

vanishing time derivatives, one may eliminate polarizations r_i in favor of field components and write profile equations of spatial variation for fields,

$$e'_R = 2ige_R + ife_L^*, \quad e'_L = -2ige_L - ife_R^*, \quad (25)$$

$$g = g(e_R, e_L) = \gamma_+ - \gamma_- \frac{16\gamma_-^2 \tau_2^2 (|e_R|^2 + |e_L|^2)^2 + 1}{16\gamma_-^2 \tau_2^2 (|e_R|^2 + |e_L|^2)^2 + 64\tau_1 \tau_2 |e_R e_L|^2 + 1}, \quad (26)$$

$$f = f(e_R, e_L) = \frac{4\tau_2 e_R e_L ((4\gamma_- \tau_2 (|e_R|^2 + |e_L|^2) - i))}{16\gamma_-^2 \tau_2^2 (|e_R|^2 + |e_L|^2)^2 + 64\tau_1 \tau_2 |e_R e_L|^2 + 1}, \quad (27)$$

$$r_3 = -\frac{16\gamma_-^2 \tau_2^2 (|e_R|^2 + |e_L|^2)^2 + 1}{16\gamma_-^2 \tau_2^2 (|e_R|^2 + |e_L|^2)^2 + 64\tau_1 \tau_2 |e_R e_L|^2 + 1}, \quad (28)$$

where $'$ indicates the spatial derivative ∂_ξ .

Despite of complicated field dependent coefficient functions that appear in f, g , the structure of profile equation (25) is rather simple. Oscillatory behavior governed by terms $\propto g$ can be eliminated by taking three bilinear forms of fields, $|e_R|^2, |e_L|^2, e_R e_L$:

$$(|e_R|^2 + |e_L|^2)' = 0, \quad (|e_R|^2 - |e_L|^2)' = -4\Im(fe_R^* e_L^*), \quad (e_R e_L)' = -if(|e_R|^2 - |e_L|^2), \quad (29)$$

where the function f depends effectively on $e_R e_L$ alone since the total flux is a constant of integration due to the first equation of (29), hence with a real constant e_0 , $|e_R(\xi)|^2 + |e_L(\xi)|^2 = e_0^2$. The set of profile equations, (29), is transformed into two equations of phase functions, $\varphi(\xi), S(\xi)$, defined by

$$e_R(\xi) = e_0 \cos \varphi(\xi), \quad e_L(\xi) = e_0 e^{iS(\xi)} \sin \varphi(\xi), \quad (30)$$

$$\varphi' = \frac{2e_0^2 \tau_2}{1 + 16\gamma_-^2 e_0^4 \tau_2^2 + 16e_0^4 \tau_1 \tau_2 \sin^2(2\varphi)} \sin(2\varphi), \quad (31)$$

$$S' = \frac{16\gamma_- e_0^2 \tau_2^2}{1 + 16\gamma_-^2 e_0^4 \tau_2^2 + 16e_0^4 \tau_1 \tau_2 \sin^2(2\varphi)} \cos(2\varphi), \quad (32)$$

with $\varphi(l/2) = \pi/4, S(l/2) = 0, l = \alpha_m L$. Since e_i 's contain four real functions, the resulting two equations here reflects a non-trivial self-consistency of the ansatz (30). A similar equation with $R \leftrightarrow L$ interchanged may be set up, suggesting another kind of solitons.

Equation for the angle function $\varphi(\xi)$ (31) is self-contained, and has the following analytic solution under the boundary condition $e_R(l/2) = e_0/\sqrt{2}$:

$$2e_R^2 - e_0^2 + \frac{16\gamma_-^2 \tau_2^2 e_0^4 + 1}{32\tau_1 \tau_2 e_0^4} \ln \frac{e_R^2}{e_0^2 - e_R^2} = -\frac{\xi - l/2}{4\tau_1}. \quad (33)$$

Field may decrease exponentially in the central region, like $e_R^2 \propto \exp[-8\tau_2 e_0^4 |\xi - l/2| / (16\gamma_-^2 \tau_2^2 e_0^4 + 1)]$. One may define the soliton size by the e-folding factor as $\xi_s = (16\gamma_-^2 \tau_2^2 e_0^4 + 1) / (8\tau_2 e_0^4)$. The actual soliton size is $x_s = \xi_s / \alpha_m$.

The spatial variation of $e_R \propto \cos \varphi(\xi)$ is monotonic, decreasing or increasing depending on the φ region of either $[0, \pi/2]$ or $[\pi/2, \pi]$ (defined modulo π). These two fundamental regions are separated since $\varphi' = 0$ at edges of these regions due to $\sin(2\varphi) = 0$ there. One may identify these two solutions as different objects. Either of fields e_R, e_L vanishes at edges of fundamental regions, but not both. Solution defined by the fundamental region $[0, \pi/2]$ corresponds to absorber soliton in which both R- and L-fluxes are absorbed at edges, but not emitted at the other edges, as illustrated in Fig(14) and Fig(15). This object may be called absorber soliton. The other fundamental region $[\pi/2, \pi]$ gives emitter soliton which may be realized when the excited $|e\rangle$ state is sufficiently occupied. The existence of two types of soliton condensates is an important result indicating existence of a new kind of topological soliton whose topology is discussed in Appendix C.

When the target size L is large and $L \gg \xi_s / \alpha_m$, one may expect a copious production of absorbers and emitters within the target. When the target size is smaller than ξ_s / α_m , the target edge effect becomes important (in general destroying, or blocking its formation of, soliton), and it may be difficult to create a soliton.

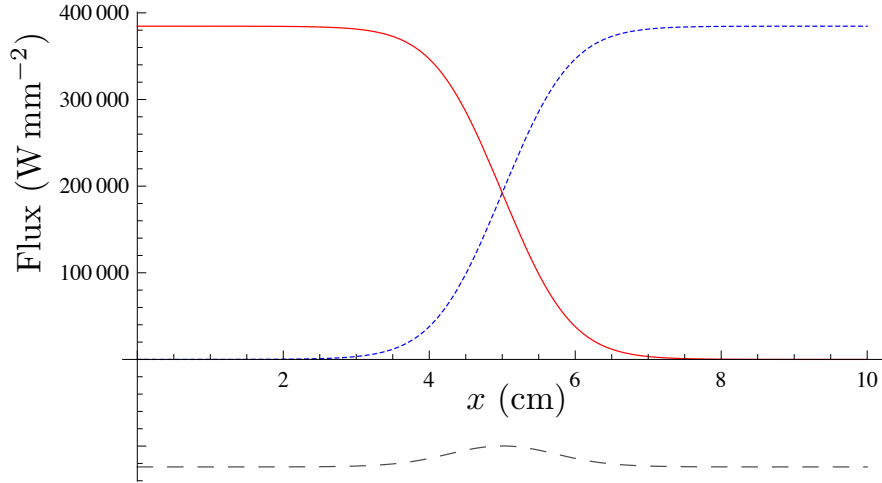


FIG. 14: (Color online) Profile of fields and r_3 of helical absorber soliton. $|E_R|^2$ (in red), $|E_L|^2$ (in dotted blue), both in the unit Wmm^{-2} , and r_3 in arbitrary unit (in dashed black) are plotted for a case of $n = 2.6 \times 10^{22} \text{cm}^{-3}$, $T_2 = 20 \text{ns}$, $T_1 = 10^3 \text{ns}$. $r_3 \approx -1$ near edges and $r_3 \approx -0.8$ in the middle.

Soliton solution obtained by direct numerical integration of (31) is illustrated in Fig(14) along with distribution of the population difference r_3 . Solitons are characterized by two end points of $r_3 \approx -1$ and an intermediate region of $r_3 \approx 0$. It is important to have a long enough target in order to accommodate many solitons within the target. Soliton size can be made smaller if one can use a larger target number density close to the solid density.

VI. CONCLUSION

In summary, we derived and numerically solved the master equation for time evolution of PSR emission and formation of field condensates in long dense targets. We have demonstrated (1) numerical identification of two different types of PSR events, explosive and weak ones, and (2) theoretical existence of spinorial solitons stable against PSR emission. Realistic experiments can be designed using numerical solutions of our master equation.

Note added.

Recently, we became aware of a related work [26] where the time evolution of triggered two-photon coherence is examined. The authors of [26] treat the field differently from the one of our semi-classical approach, which results in our coherence development time of order several nano seconds in dense targets, much shorter than their value.

Acknowledgments

This research was partially supported by Grant-in-Aid for Scientific Research on Innovative Areas "Extreme quantum world opened up by atoms" (21104002) from the Ministry of Education, Culture, Sports, Science, and Technology.

Appendix A: Two level effective model interacting with multi-mode fields

We extend results of Appendix A in [14] to the case of multi-mode fields such that two color problem including propagation effect is properly treated. This is the most general case of two photon problem. Its notation in this reference is slightly changed.

Atomic system

The state vector of an atom can be expanded in terms of the wave function,

$$|\psi(t)\rangle = c_g(t)e^{-i\epsilon_g t}|g\rangle + c_e(t)e^{-i\epsilon_e t}|e\rangle + \sum_p c_p(t)e^{-i\epsilon_p t}|p\rangle. \quad (\text{A1})$$

$c_a(t)$'s are probability amplitudes in an interaction picture where ϵ_a 's are energies of atomic states.

The atomic system may interact with light fields. The electric field $E(x, t)$ that appears in the hamiltonian via E1 or M1 transition is assumed to have one vector component alone, namely we ignore effects of field polarization. This is a valid approach under a number of circumstances. One then decomposes the real field variable $E(x, t)$ into Fourier series, $e^{-i\omega_j t}$ times a complex envelope amplitude $E_j(x, t)$, and its conjugate, where $E_j(x, t)$ is assumed slowly varying in time,

$$E(x, t) = \sum_j (E_j^*(x, t)e^{i\omega_j t} + E_j(x, t)e^{-i\omega_j t}). \quad (\text{A2})$$

Each discrete mode j is taken independent. The most interesting are the cases of two modes with $\omega_1 + \omega_2 = \epsilon_{eg}$ and the single mode with $\omega = \epsilon_{eg}/2$.

The Schrödinger equation for a single atom,

$$i\frac{\partial}{\partial t}|\psi(t)\rangle = (H_0 + dE)|\psi(t)\rangle, \quad (\text{A3})$$

with H_0 the atomic hamiltonian, is used to derive the upper level amplitude $c_p(t)$. Using

$$i\frac{\partial}{\partial t}\langle p|\psi(t)\rangle = \langle p|(H_0 + dE)|\psi(t)\rangle, \quad (\text{A4})$$

one has

$$i\frac{dc_p}{dt}e^{-i\epsilon_p t} = (d_{pe}c_e e^{-i\epsilon_e t} + d_{pg}c_g e^{-i\epsilon_g t})E, \quad (\text{A5})$$

where d_{ab} are dipole matrix elements. This can formally be integrated to

$$\begin{aligned} c_p(t) &= -i \int_0^t dt' \left(d_{pe}c_e(t')e^{i\epsilon_{pe}t'} + d_{pg}c_g(t')e^{i\epsilon_{pg}t'} \right) E(x, t') \\ &= -i \int_0^t dt' \sum_j \left(d_{pe}c_e(t')e^{i\epsilon_{pe}t'} + d_{pg}c_g(t')e^{i\epsilon_{pg}t'} \right) \left(E_j^*(x, t')e^{i\omega_j t'} + E_j(x, t')e^{-i\omega_j t'} \right), \end{aligned} \quad (\text{A6})$$

with $\epsilon_{ab} = \epsilon_a - \epsilon_b$ the atomic level energy difference. The initial condition $c_p(0) = 0$ is assumed here.

Markovian approximation and effective two level model

The basic strategy of deriving equations for the lower two level amplitudes c_e, c_g in a closed form is to eliminate atomic variables c_p 's related to the upper levels. This is essentially done by neglecting a long-time memory effect (the Markovian approximation) and making slowly varying envelope approximation (SVEA). The idea of the Markovian approximation is to replace dynamical variables, $c_e(t'), c_g(t'), E_j(x, t')$ in the integrand of eq.(A6), by their values at time t , neglecting all the past memory effects. This gives

$$c_p(t) \approx \sum_j d_{pe} c_e \left(\frac{1 - e^{i(\omega_j + \epsilon_{pe})t}}{\omega_j + \epsilon_{pe}} E_j^* - \frac{1 - e^{-i(\omega_j - \epsilon_{pe})t}}{\omega_j - \epsilon_{pe}} E_j \right) + d_{pg} c_g \left(\frac{1 - e^{i(\omega_j + \epsilon_{pg})t}}{\omega_j + \epsilon_{pg}} E_j^* - \frac{1 - e^{-i(\omega_j - \epsilon_{pg})t}}{\omega_j - \epsilon_{pg}} E_j \right), \quad (\text{A7})$$

which is inserted into equations for the lower levels

$$\frac{dc_e}{dt} = -i \sum_p d_{ep} E(x, t) c_p(t) e^{-i\epsilon_{pe}t}, \quad (\text{A8})$$

$$\frac{dc_g}{dt} = -i \sum_p d_{gp} E(x, t) c_p(t) e^{-i\epsilon_{pg}t}. \quad (\text{A9})$$

Note that $d_{ab} = d_{ba}$ are real by an appropriate choice of phases.

We ignore rapidly oscillating terms, keeping in mind the two most important cases of the mode choice. The result is

$$\frac{d}{dt} \begin{pmatrix} c_e \\ c_g \end{pmatrix} = -i \mathcal{H}_I \begin{pmatrix} c_e \\ c_g \end{pmatrix}, \quad (\text{A10})$$

$$- \mathcal{H}_I = \sum_{jj'} \begin{pmatrix} \mu_{ee}(\omega_j, \omega_{j'}) e^{i(\omega_j - \omega_{j'})t} E_j^* E_{j'} & e^{-i(\omega_j + \omega_{j'} - \epsilon_{eg})t} \mu_{eg}(\omega_j, \omega_{j'}) E_j E_{j'} \\ e^{i(\omega_j + \omega_{j'} - \epsilon_{eg})t} \mu_{ge}(\omega_j, \omega_{j'}) E_j^* E_{j'} & \mu_{gg}(\omega_j, \omega_{j'}) e^{i(\omega_j - \omega_{j'})t} E_j^* E_{j'} \end{pmatrix} \quad (\text{A11})$$

$$\equiv \mathcal{E}_j \mathcal{M}_{jj'} \mathcal{E}_{j'},$$

$$\mu_{ee}(\omega_j, \omega_{j'}) = \sum_p \frac{d_{pe}^2 (2\epsilon_{pe} + \omega_j - \omega_{j'})}{(\epsilon_{pe} + \omega_j)(\epsilon_{pe} - \omega_{j'})}, \quad \mu_{gg}(\omega_j, \omega_{j'}) = \sum_p \frac{d_{pg}^2 (2\epsilon_{pg} + \omega_j - \omega_{j'})}{(\epsilon_{pg} + \omega_j)(\epsilon_{pg} - \omega_{j'})}, \quad (\text{A12})$$

$$\mu_{eg}(\omega_j, \omega_{j'}) = \sum_p \frac{d_{pe} d_{pg} (\epsilon_{pg} - (\omega_j + \omega_{j'})/2)}{(\epsilon_{pg} - \omega_j)(\epsilon_{pg} - \omega_{j'})}, \quad \mu_{ge}(\omega_j, \omega_{j'}) = \sum_p \frac{d_{pe} d_{pg} (\epsilon_{pe} + (\omega_j + \omega_{j'})/2)}{(\epsilon_{pe} + \omega_j)(\epsilon_{pe} + \omega_{j'})}. \quad (\text{A13})$$

\mathcal{E} may contain both E_j and E_j^* . We simplify notations below such that fields are redefined incorporating oscillating factors $e^{-i\omega_j t}$ in E_j^+ etc.

Single color problem

We apply the result to the problem of counter-propagating fields E_R and E_L of a single color of $\omega_0 = \epsilon_{eg}/2$. In the 2×2 hamiltonian (A11) one may use the complex field $E^+ \equiv E_j e^{-i\omega_j t}$ (the positive energy component corresponding to the photon annihilation operator) and its conjugate $E^- \equiv E_j^* e^{i\omega_j t}$ (the negative energy component corresponding to the photon creation operator) to eliminate phase factors except $e^{\pm i\epsilon_{eg}t}$, as is done in the main text. Since each mode is independent, it separately satisfies the field commutation relation, necessary for derivation of the quantum field equation, justifying the result of manuscript for the degenerate case.

More concretely,

$$-\mathcal{H}_I = \begin{pmatrix} \mu_{ee}(E_R^+ E_R^- + E_L^+ E_L^- + E_R^+ E_L^- + E_L^+ E_R^-) & e^{i\epsilon_{eg}t} \mu_{ge}(E_R^+ E_R^+ + E_L^+ E_L^+ + 2E_R^+ E_L^+) \\ e^{-i\epsilon_{eg}t} \mu_{ge}(E_R^- E_R^- + E_L^- E_L^- + 2E_R^- E_L^-) & \mu_{gg}(E_R^+ E_R^- + E_L^+ E_L^- + E_R^+ E_L^- + E_L^+ E_R^-) \end{pmatrix}, \quad (\text{A14})$$

$$\mu_{ge} = \frac{2d_{pe}d_{pg}}{\epsilon_{pg} + \epsilon_{pe}}, \quad \mu_{aa} = \frac{2d_{pa}^2 \epsilon_{pa}}{\epsilon_{pa}^2 - \omega_0^2}. \quad (\text{A15})$$

(RR) and (LL) terms describe pulse propagation with compression and splitting, while (RL) terms back-scattering, pair creation, and pair annihilation.

Two color problem

We may consider for E_R, E_L envelopes of two different colors of ω_i with $\omega_1 + \omega_2 = \epsilon_{eg}$. Separation of cross mode terms leads to

$$\mathcal{H}_I = \mathcal{H}_{d,R} + \mathcal{H}_{d,L} + \mathcal{H}_{12,R} + \mathcal{H}_{12,L} + \mathcal{H}_{12,RL}, \quad (\text{A16})$$

$$-\mathcal{H}_{d,i} = \begin{pmatrix} \sum_{i,a} \mu_{ee}(\omega_a, \omega_a) E_{i,a}^+ E_{i,a}^- & e^{i\epsilon_{eg}t} \sum_{i,a} \mu_{eg}(\omega_a, \omega_a) E_{i,a}^+ E_{i,a}^+ \\ e^{-i\epsilon_{eg}t} \sum_{i,a} \mu_{ge}(\omega_a, \omega_a) E_{i,a}^- E_{i,a}^- & \sum_{i,a} \mu_{gg}(\omega_a, \omega_a) E_{i,a}^+ E_{i,a}^- \end{pmatrix}, \quad (\text{A17})$$

$$-\mathcal{H}_{12,i} = \begin{pmatrix} \mu_{ee}(\omega_1, \omega_2) E_{i,1}^+ E_{i,2}^- + \mu_{ee}(\omega_2, \omega_1) E_{i,2}^+ E_{i,1}^- & e^{i\epsilon_{eg}t} 2\mu_{eg}(\omega_1, \omega_2) E_{i,1}^+ E_{i,2}^+ \\ e^{-i\epsilon_{eg}t} 2\mu_{ge}(\omega_1, \omega_2) E_{i,1}^- E_{i,2}^- & \mu_{gg}(\omega_1, \omega_2) E_{i,1}^+ E_{i,2}^- + \mu_{gg}(\omega_2, \omega_1) E_{i,2}^+ E_{i,1}^- \end{pmatrix}, \quad (\text{A18})$$

$$\begin{aligned} -(\mathcal{H}_{12,RL})_{aa} &= \mu_{aa}(\omega_1, \omega_2) E_{R,1}^+ E_{L,2}^- + \mu_{aa}(\omega_2, \omega_1) E_{R,2}^+ E_{L,1}^- \\ &\quad + \mu_{aa}(\omega_1, \omega_2) E_{L,1}^+ E_{R,2}^- + \mu_{aa}(\omega_2, \omega_1) E_{L,2}^+ E_{R,1}^-, \end{aligned} \quad (\text{A19})$$

$$-(\mathcal{H}_{12,RL})_{eg} = e^{i\epsilon_{eg}t} 2\mu_{eg}(\omega_1, \omega_2) (E_{R,1}^+ E_{L,2}^+ + E_{R,2}^+ E_{L,1}^+), \quad (\text{A20})$$

$$\mu_{aa}(\omega_1, \omega_2) = \frac{d_{pa}^2(2\epsilon_{pa} + \omega_1 - \omega_2)}{(\epsilon_{pa} + \omega_1)(\epsilon_{pa} - \omega_2)}, \quad (\text{A21})$$

$$\mu_{ge}(\omega, \epsilon_{eg} - \omega) = \mu_{ge}(\epsilon_{eg} - \omega, \omega) = \mu_{eg}(\omega, \epsilon_{eg} - \omega) = \mu_{eg}(\epsilon_{eg} - \omega, \omega) = \frac{d_{pe}d_{pg}(\epsilon_{pg} + \epsilon_{pe})}{(\epsilon_{pe} + \omega)(\epsilon_{pg} - \omega)}. \quad (\text{A22})$$

Bloch equation

The Bloch vector defined by

$$\vec{R} = \langle \psi | \vec{\sigma} | \psi \rangle = \text{tr } \vec{\sigma} \rho, \quad \rho = |\psi\rangle\langle\psi| = \begin{pmatrix} c_e^* c_e & c_e^* c_g \\ c_g^* c_e & c_g^* c_g \end{pmatrix}, \quad (\text{A23})$$

satisfies quantum mechanical equation (disregarding relaxation terms) $\partial_t \vec{R} = -i \text{tr } \vec{\sigma} [\mathcal{H}_I, \rho]$.

Explicit calculation using the Hamiltonian above gives

$$\partial_t R_1 = (\mu_{ee} - \mu_{gg}) E^+ E^- R_2 - i \mu_{ge} (e^{i\epsilon_{eg}t} E^+ E^+ - e^{-i\epsilon_{eg}t} E^- E^-) R_3, \quad (\text{A24})$$

$$\partial_t R_2 = -(\mu_{ee} - \mu_{gg}) E^+ E^- R_1 + \mu_{ge} (e^{i\epsilon_{eg}t} E^+ E^+ + e^{-i\epsilon_{eg}t} E^- E^-) R_3, \quad (\text{A25})$$

$$\partial_t R_3 = \mu_{ge} (i(e^{i\epsilon_{eg}t} E^+ E^+ - e^{-i\epsilon_{eg}t} E^- E^-) R_1 - (e^{i\epsilon_{eg}t} E^+ E^+ + e^{-i\epsilon_{eg}t} E^- E^-) R_2). \quad (\text{A26})$$

We suppressed mode index j for simplicity. Conservation law holds: $\partial_t (R_1^2 + R_2^2 + R_3^2) = 0$.

Field equation

Commutation relation of fields necessary for derivation of quantum field equation $[E_y(\vec{r}, t), B_z(\vec{r}', t)] = i \partial_x \delta^3(\vec{r} - \vec{r}')$, is valid for each independent mode. The double commutator,

$$\partial_t^2 \vec{E}^\pm = -[H, [H, \vec{E}^\pm]], \quad H = \int d^3x (\mathcal{H}_f + \text{tr } \rho \mathcal{H}_I), \quad (\text{A27})$$

$$\text{tr } \rho \mathcal{H}_I = \langle \psi | \mathcal{H} | \psi \rangle = -(\mu_{ee} |c_e|^2 + \mu_{gg} |c_g|^2) E^+ E^- - \mu_{ge} (c_e^* c_g E^+ E^+ + c_g^* c_e E^- E^-), \quad (\text{A28})$$

with the field energy density $\mathcal{H}_f = (\vec{E}^2 + \vec{B}^2)/2$, is calculated as

$$(\partial_t^2 - \vec{\nabla}^2) \vec{E}_j^\pm = \vec{\nabla}^2 (\mathcal{D}_{jj'} \vec{E}_{j'}^\pm), \quad (\text{A29})$$

$$-\mathcal{D}_{jj'} \vec{E}_{j'}^\pm = \left(\frac{(\mu_{ee} + \mu_{gg})_{jj'}}{2} n + \frac{(\mu_{ee} - \mu_{gg})_{jj'}}{2} R_3 \right) \vec{E}_{j'}^\pm + (\mu_{ge})_{jj'} e^{-i\epsilon_{eg}t} (R_1 - iR_2) \vec{E}_{j'}^\mp. \quad (\text{A30})$$

SVEA and dimensionless equations for two color modes

All terms both in the Bloch and field equations must have the same oscillatory behavior for global evolution of polarization and fields. This gives a phase matching condition of the

form $\omega_1 + \omega_2 = \epsilon_{eg}$ and momentum balance with $E_R \propto e^{i\omega x}$, $E_L \propto e^{-i\omega x}$. For time SVEA one may then eliminate the phase factor $e^{\pm i\epsilon_{eg}t}$ in the Bloch equation. For space SVEA we introduce spatial variation of polarization of the form,

$$R_i = R_i^{(0)} + R_i^{(+)} e^{2i\omega x} + R_i^{(-)} e^{-2i\omega x}. \quad (\text{A31})$$

LHS of field equations $\sim -2i\omega(\partial_t \pm \partial_x)E_{R,L}$ for the counter-propagating modes of the same frequency, hence (with $\partial_{\pm} \equiv \partial_t \pm \partial_x$)

$$\begin{aligned} \partial_+ E_R = \frac{i\omega}{2} & \left(\left(\frac{\mu_{ee} + \mu_{gg}}{2} n + \frac{\mu_{ee} - \mu_{gg}}{2} R_3^{(0)} \right) E_R + \frac{\mu_{ee} - \mu_{gg}}{2} R_3^{(+)} E_L \right. \\ & \left. + \mu_{ge} \left((R_1 - iR_2)^{(0)} E_L^* + (R_1 - iR_2)^{(+)} E_R^* \right) \right), \end{aligned} \quad (\text{A32})$$

$$\begin{aligned} \partial_- E_L = \frac{i\omega}{2} & \left(\left(\frac{\mu_{ee} + \mu_{gg}}{2} n + \frac{\mu_{ee} - \mu_{gg}}{2} R_3^{(0)} \right) E_L + \frac{\mu_{ee} - \mu_{gg}}{2} R_3^{(-)} E_R \right. \\ & \left. + \mu_{ge} \left((R_1 - iR_2)^{(0)} E_R^* + (R_1 - iR_2)^{(-)} E_L^* \right) \right). \end{aligned} \quad (\text{A33})$$

We introduce the dimensionless unit:

$$(\xi, \tau) = (\alpha_m x, \alpha_m t), \quad \alpha_m(\omega) = \frac{\epsilon_{eg}}{2} n \mu_{ge}(\omega, \epsilon_{eg} - \omega), \quad |e_{L,R}^{(1),(2)}|^2 = \frac{|E_{L,R}^{(1),(2)}|^2}{\epsilon_{eg} n}, \quad r_i = \frac{R_i}{n}. \quad (\text{A34})$$

Assume R-mover of frequency ω_1 and L-mover of frequency ω_2 (neither R-mover of frequency ω_2 nor L-mover of frequency ω_1). Note the universal parameter $\mu_{eg}(\omega_1, \omega_2) = \mu_{ge}(\omega_1, \omega_2)$ for any combination of $\omega_1 + \omega_2 = \epsilon_{eg}$. The master equations for medium polarization and fields are

$$\begin{aligned} \partial_{\tau} r_1^{(0)} = & 4(\gamma_-^{(1)} |e_R|^2 + \gamma_-^{(2)} |e_L|^2) r_2^{(0)} + 8\Im(e_R e_L) r_3^{(0)} + 4\gamma_-^{(12)} e_R e_L^* r_2^{(-)} + 4\gamma_-^{(21)} e_L e_R^* r_2^{(+)} \\ & - 2i(e_L^2 - (e_R^*)^2) r_3^{(+)} - 2i(e_R^2 - (e_L^*)^2) r_3^{(-)} - \frac{r_1^{(0)}}{\tau_2}, \end{aligned} \quad (\text{A35})$$

$$\partial_{\tau} r_1^{(+)} = 4\gamma_-^{(12)} e_R e_L^* r_2^{(0)} - 2i(e_R^2 - (e_L^*)^2) r_3^{(0)} + 4(\gamma_-^{(1)} |e_R|^2 + \gamma_-^{(2)} |e_L|^2) r_2^{(+)} + 8\Im(e_R e_L) r_3^{(+)} - \frac{r_1^{(+)}}{\tau_2}, \quad (\text{A36})$$

$$\begin{aligned} \partial_{\tau} r_2^{(0)} = & -4(\gamma_-^{(1)} |e_R|^2 + \gamma_-^{(2)} |e_L|^2) r_1^{(0)} + 8\Re(e_R e_L) r_3^{(0)} - 4\gamma_-^{(12)} e_R e_L^* r_1^{(-)} - 4\gamma_-^{(21)} e_L e_R^* r_1^{(+)} \\ & + 2(e_L^2 + (e_R^*)^2) r_3^{(+)} + 2(e_R^2 + (e_L^*)^2) r_3^{(-)} - \frac{r_2^{(0)}}{\tau_2}, \end{aligned} \quad (\text{A37})$$

$$\partial_{\tau} r_2^{(+)} = -4\gamma_-^{(12)} e_R e_L^* r_1^{(0)} + 2(e_R^2 + (e_L^*)^2) r_3^{(0)} - 4(\gamma_-^{(1)} |e_R|^2 + \gamma_-^{(2)} |e_L|^2) r_1^{(+)} + 8\Re(e_R e_L) r_3^{(+)} - \frac{r_2^{(+)}}{\tau_2}, \quad (\text{A38})$$

$$\begin{aligned} \partial_\tau r_3^{(0)} &= -8 \left(\Re(e_R e_L) r_2^{(0)} + \Im(e_R e_L) r_1^{(0)} \right) + 2i(e_R^2 - (e_L^*)^2) r_1^{(-)} + 2i(e_L^2 - (e_R^*)^2) r_1^{(+)} \\ &\quad - 2(e_L^2 + (e_R^*)^2) r_2^{(+)} - 2(e_R^2 + (e_L^*)^2) r_2^{(-)} - \frac{r_3^{(0)} + 1}{\tau_1}, \end{aligned} \quad (\text{A39})$$

$$\partial_\tau r_3^{(+)} = 2ir_1^{(0)}(e_R^2 - (e_L^*)^2) - 2r_2^{(0)}(e_R^2 + (e_L^*)^2) - 8 \left(\Re(e_R e_L) r_2^{(+)} + \Im(e_R e_L) r_1^{(+)} \right) - \frac{r_3^{(+)}}{\tau_1}, \quad (\text{A40})$$

$$(\partial_\tau + \partial_\xi) e_R = \frac{ia_1}{2} (\gamma_+^{(1)} + \gamma_-^{(1)} r_3^{(0)}) e_R + \frac{i}{2} \gamma_-^{(12)} r_3^{(+)} e_L + \frac{ia_{12}}{2} (r_1^{(0)} - ir_2^{(0)}) e_L^* + \frac{i}{2} (r_1^{(+)} - ir_2^{(+)}) e_R^*, \quad (\text{A41})$$

$$(\partial_\tau - \partial_\xi) e_L = \frac{ia_2}{2} (\gamma_+^{(2)} + \gamma_-^{(2)} r_3^{(0)}) e_L + \frac{i}{2} \gamma_-^{(21)} r_3^{(-)} e_R + \frac{ia_{21}}{2} (r_1^{(0)} - ir_2^{(0)}) e_R^* + \frac{i}{2} (r_1^{(-)} - ir_2^{(-)}) e_L^*. \quad (\text{A42})$$

$$\gamma_\pm^{(a)} = \frac{\mu_{ee}(\omega_a, \omega_a) \pm \mu_{gg}(\omega_a, \omega_a)}{2\mu_{ge}}, \quad \gamma_\pm^{(ab)} = \frac{\mu_{ee}(\omega_a, \omega_b) \pm \mu_{gg}(\omega_a, \omega_b)}{2\mu_{ge}}, \quad (\text{A43})$$

$$a_i = \frac{2\omega_i}{\epsilon_{eg}}, \quad a_{ij} = \frac{2\omega_j^2}{\omega_i \epsilon_{eg}}, \quad (\text{A44})$$

with μ_{ab} defined by (A15).

The single mode equations in the text are readily derived by taking $\omega_i = \epsilon_{eg}/2$, $a_i = 1$, $a_{ij} = 1$ and all $\gamma_\pm^{(ab)}$ a, b -independent.

Pulse compression factor

We shall estimate pulse propagation effects neglected in the text. Pulse propagation may be described by ignoring RL mixing terms in the general master equations. By taking one mode e_R of one color, the basic propagation equations are

$$\partial_\tau r_1 = 4r_3 \Im e_R^2 + 4\gamma_- r_2 |e_R|^2 - \frac{r_1}{\tau_2}, \quad (\text{A45})$$

$$\partial_\tau r_2 = 4r_3 \Re e_R^2 - 4\gamma_- r_1 |e_R|^2 - \frac{r_2}{\tau_2}, \quad (\text{A46})$$

$$\partial_\tau r_3 = -4(r_1 \Im e_R^2 + r_2 \Re e_R^2) - \frac{r_3 + 1}{\tau_1}, \quad (\text{A47})$$

$$(\partial_\tau + \partial_\xi) e_R = \frac{i}{2} ((\gamma_+ + \gamma_- r_3) e_R + (r_1 - ir_2) e_R^*). \quad (\text{A48})$$

We shall ignore relaxation terms, taking $\tau_i \rightarrow \infty$. Results of [14] in terms of the area function follow with the assumption of reality of the function e_R . The relation $r_1 = -\gamma_- r_3$ automatically follows from the consistency of three Bloch equations. The fundamental equation of the propagation problem is given by a single non-linear field equation in terms of the

area function $\theta(\xi, \tau)$:

$$e_R^2 = \frac{\partial_\tau \theta}{4\sqrt{1 + \gamma_-^2}}, \quad r_3 = \pm \frac{\cos \theta}{\sqrt{1 + \gamma_-^2}}, \quad r_2 = \pm \sin \theta, \quad (\text{A49})$$

$$(\partial_\tau + \partial_\xi)\partial_\tau \theta = \pm \sin \theta \partial_\tau \theta. \quad (\text{A50})$$

Analytic solutions of this non-linear equation give [14]

(1) Pulse splitting. The number N of split pulses is given by the pulse area of the initial flux $F_i(t)$ divided by 2π :

$$N = \frac{1}{2\pi} \sqrt{\mu_{ge}^2 + (\mu_{ee} - \mu_{gg})^2/4} \int_{-\infty}^{\infty} dy F_i(y). \quad (\text{A51})$$

(2) Pulse compression. The pulse of area $< 2\pi$ is compressed by an amount E (result obtained for Lorentzian pulse),

$$E = \frac{1}{(\alpha_m x \sin(\tilde{\theta}/2) \pm \cos(\tilde{\theta}/2))^2 + \sin^2(\tilde{\theta}/2)}, \quad (\text{A52})$$

$$\tilde{\theta} = \sqrt{\mu_{ge}^2 + (\mu_{ee} - \mu_{gg})^2/4} \int_{-\infty}^{t-x} dy F_i(y), \quad (\text{A53})$$

\pm depending on amplifier (absorber).

We may estimate the pulse compression factor (A52) for CW trigger irradiation of duration t in which case $\tilde{\theta} \sim \beta t$:

$$E = \frac{1}{(\beta t \alpha_m x \pm 1)^2 + (\beta t)^2} \sim \frac{1}{1 \pm 2\beta t \alpha_m x}. \quad (\text{A54})$$

In all cases of our interest $\beta t \leq \beta T_2 \ll 1$. Thus, unless the target length is large enough, close to $1/(2\beta T_2 \alpha_m)$, the effect of pulse compression is not large.

Appendix B: Exact and approximate conservation laws

We focus on the degenerate case of $\omega_1 = \omega_2 = \epsilon_{eg}/2$. There are three different classes of exact and approximate conservation laws: (1) one exact conservation that holds with finite T_i , (2) one more approximate conservation law that holds in the $T_1 \rightarrow \infty$ limit, (3) one further approximate conservation law that holds in the $T_2 \rightarrow \infty$ limit ($T_1 \gg T_2$ assumed).

The first exact conservation law is derived directly from two equations of motion for the field e_i and it reads as

$$(\partial_\tau + \partial_\xi)|e_R|^2 = (\partial_\tau - \partial_\xi)|e_L|^2. \quad (\text{B1})$$

An integral form of this conservation for a finite target of length L ($l = \alpha_m L$ below) is

$$\frac{d}{d\tau} \int_0^l d\xi (|e_R|^2 - |e_L|^2) = -[|e_R|^2 + |e_L|^2]_{\xi=0}^l. \quad (\text{B2})$$

The integrated quantity of $|e_R|^2 - |e_L|^2$ stored in the target balances against its flux outgoing from two target ends. For the symmetric trigger, RHS of this equation vanishes, and the integral in LHS is a constant of motion.

The second conservation law that holds in the $T_1 \rightarrow \infty$ limit is

$$\partial_\tau (r_3 + 4(|e_R|^2 + |e_L|^2)) + 4\partial_\xi (|e_R|^2 - |e_L|^2) = 0, \quad (\text{B3})$$

corresponding to the energy conservation. The energy density inside the target is a sum of medium and field energies, $r_3/2 + 2(|e_R|^2 + |e_L|^2)$, in our dimensionless unit. The integrated form of this conservation law in the real unit is

$$\frac{d}{dt} \int_0^L dx \left(\frac{\epsilon_{eg}}{2} R_3 + 2(|E_R|^2 + |E_L|^2) \right) = -2[|E_R|^2 - |E_L|^2]_{x=0}^L. \quad (\text{B4})$$

The third class of conservation law that holds in the $T_2 \rightarrow \infty$ limit is

$$\partial_\tau (r_1^2 + r_2^2 + r_3^2) = 0. \quad (\text{B5})$$

Appendix C: Helical soliton

A new type of topological solitons may exist, because the basic equation has two components $\varphi^{(i)}(\xi)$, $i = 1, 2$, and one can give a topological quantum number in 1+1 dimensions, as illustrated in Fig(15). For simplicity assume two real component field (X, Y) and its periodicity with period of the target length $l (= \alpha_m L)$ or a few times of this length. We may define the homotopy class [27] of the mapping of a circle $x + iy = le^{i\xi}$, $0 \leq \xi \leq 2\pi$ in two dimensional real space onto the field space of the unit magnitude, $X^2 + Y^2 = 1$. The winding number w is defined using the complex field $Z = X + iY = e^{i\varphi(\xi)}$:

$$w = -i \int_0^{2\pi} \frac{d\xi}{2\pi} Z^* \partial_\xi Z = \frac{\varphi(2\pi) - \varphi(0)}{2\pi}. \quad (\text{C1})$$

When this winding number is quantized, $w = n$, $n = 0, \pm 1, \pm 2, \dots$, the winding number is topologically stable and conserved during time evolution.

The correspondence to static solutions in Section V is as follows. One considers the real 3-vector field $\vec{X}(\xi)$ of unit length, $(X, Y, Z) = (\cos \varphi, \cos S \sin \varphi, \sin S \sin \varphi)$ with φ, S

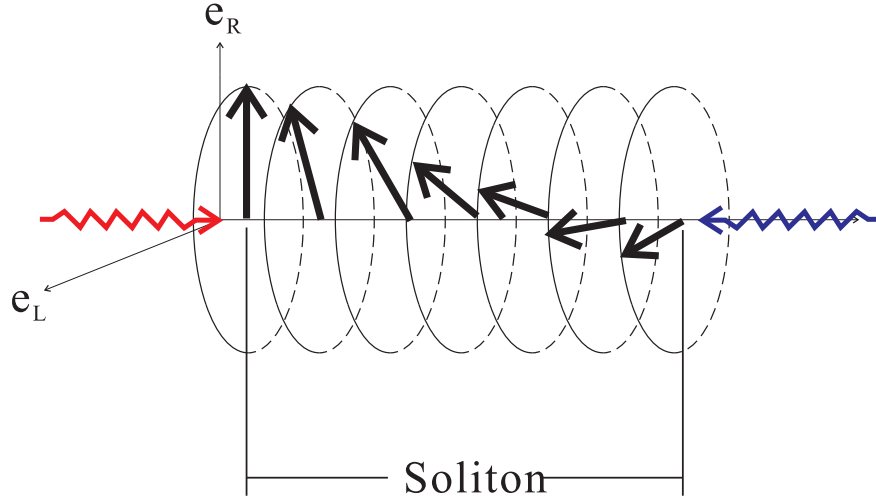


FIG. 15: (Color online) Helical structure of absorber soliton. Target region is irradiated from both ends by trigger lasers of different colors. The $\vec{X}(\xi) = (\cos \varphi, \cos S \sin \varphi, \sin S \sin \varphi)$ with φ, S defined by eq.(30) may wind. In the return trip from the right edge to the left edge, not shown here, $\vec{X}(\xi)$ further winds and comes back with $\vec{X}(\pi) = -\vec{X}(0)$ at the left edge, giving a spinor field. This is an absorber soliton without emission at two ends.

identified as the phase variables in static solutions, and a mapping of unit circle $0 \leq \xi \leq 2\pi$ onto $\vec{X}(\xi)$ space. Two solutions of eq.(31), (32) corresponding to two different fundamental regions, $[0, \pi/2]$ and $[\pi/2, \pi]$, are connected together at $\xi = \pi/2$. Then, in the return trip of $\xi = \pi/2 \rightarrow \pi$ from the right edge to the left edge of soliton, the orientation of $\vec{X}(\xi)$ is further advanced forward (dictated by continuity of solutions), and finally comes back with $\vec{X}(\pi) = -\vec{X}(0)$ at the left edge. This means that solutions of \vec{X} are two-valued representation, namely spinors.

-
- [1] P.P. Sorokin and N. Braslau, IBM J. Phys. Rev. **8**, 177 (1964); R.L. Garwin, IBM J. Phys. Rev. **8**, 338 (1964); A.M. Prokhorov, Science **149**, 828 (1965).
 - [2] E.M. Belenov and I.A. Poluektov, Zh. Eksp. Teor. Fiz. **56**, 1407 (1969) [Sov. Phys. JETP **29**, 754 (1969)].
 - [3] L.M. Narducci, W.W. Eidson, P. Furciniti, and D.C. Eteson, Phys. Rev. A **16**, 1665 (1977).
 - [4] S.E. Harris, J.E. Field, and A. Imamoglu, Phys. Rev. Lett. **64**, 1107 (1990).
 - [5] R.L. Shoemaker and R.G. Brewer, Phys. Rev. Lett. **28**, 1430 (1972).

- [6] N. Tan-no, K. Yokoto, and H. Inaba, Phys. Rev. Lett. **29**, 1211 (1972).
- [7] M. Brune, J.M. Raimond, P. Goy, L. Davidovich, and S. Haroche, Phys. Rev. Lett. **17**, 1899 (1987).
- [8] For a review of experimental and theoretical aspects of EIT, see M. Fleischhauer, A. Imamoglu, and J.P. Marangos, Rev. Mod. Phys. **77**, 633 (2005).
- [9] D.J. Gauthier, Q. Wu, S.E. Morin, and T.W. Mossberg, Phys. Rev. Lett. **68**, 464 (1992).
- [10] M. Yoshimura, C. Ohae, A. Fukumi, K. Nakajima, I. Nakano, H. Nanjo, and N. Sasao, *Macro-coherent two photon and radiative neutrino pair emission*, arXiv:0805.1970 [hep-ph] (2008); M. Yoshimura, *Neutrino Spectroscopy using Atoms (SPAN)*, in Proceedings of 4th NO-VE International Workshop, edited by M. Baldo Ceolin (2008).
- [11] For a review of both the theory and experiments of superradiance, M. Benedict, A.M. Ermolaev, V.A. Malyshev, I.V. Sokolov, and E.D. Trifonov, *Super-radiance: Multiatomic coherent emission* (Taylor & Francis Group, New York, 1996); For a formal aspect of the theory, M. Gross and S. Haroche, Phys. Rep. **93**, 301 (1982); The original suggestion of superradiance is due to R.H. Dicke, Phys. Rev. **93**, 99 (1954).
- [12] F. Haake, H. King, G. Schöder, J. Haus, and R. Glauber, Phys. Rev. A **20**, 2047 (1979). D. Polder, M.F.H. Schuurmans, and Q.H.F. Vreken, Phys. Rev. A **19**, 1192 (1979).
- [13] Q.H.F. Vreken and M.F.H. Schuurmans, Phys. Rev. Lett. **42**, 224 (1979). N.W. Carlson *et al.*, Opt. Commun. **32**, 350 (1980).
- [14] M. Yoshimura, Prog. Theor. Phys. **125**, 149 (2011).
- [15] M. Yoshimura, Phys. Lett. B **699**, 123 (2011); Phys. Rev. D **75**, 113007 (2007).
- [16] S.L. McCall and E.L. Hahn, Phys. Rev. **183**, 457 (1969); For a review, L. Allen and J.H. Eberly, *Optical Resonance and Two-level Atoms* (Dover, New York, 1975); For comparison with experimental results, R.E. Slusher and H.M. Gibbs, Phys. Rev. A **4**, 1634 (1972).
- [17] D.D. Yavuz, Phys. Rev. A **75**, 041802(R) (2007) and references therein.
- [18] W. Kolos and L. Wolniewicz, J. Chem. Phys. **46**, 1426 (1967).
- [19] The parameter μ_{ab} may also be estimated from E1 coupling data of electronically excited $B \rightarrow X$ transition including Franck-Condon vibrational overlap factors, given by calculation of U. Frantz and D. Wunderlich, *Franck-Condon Factors, Transition Probabilities, and Radiative Lifetimes for Hydrogen Molecules and Their Isotopomers*, INDC(NDS)-457. This estimate gives consistent result with the polarizability of [18].

- [20] G. Lindblad, *Comm. Math. Phys.* **48**, 119 (1976).
- [21] J.J. Sakurai, *Advanced Quantum Mechanics* (Addison-Wesley, 1967).
- [22] The field equation, (9) \sim (10) and (A29) \sim (A30), may also be derived by computing macroscopic polarization vector, as is done in references [3] and [14] for the more restricted case.
- [23] M. Lewenstein and K. Rzazewski, *Phys. Rev. A* **26**, 1510 (1982).
- [24] E.R. Golubyatnikova, V.V. Kocharovskii, V.I. Kocharovskii, *Quantum Electron.* **24**, 791 (1994).
- [25] For a review of STIRAP, see K. Bergmann, H. Theuer, and B.W. Shore, *Rev. Mod. Phys.* **70**, 1003 (1998).
- [26] A.A. Kalinkin, A.A. Kalachev, and V.V. Samartsev, *Laser Phys.* **14**, 71 (2004) and references therein.
- [27] S. Coleman, *Aspects of Symmetry* (Cambridge University Press, Cambridge, UK, 1985).